A High-Order Discontinuous Galerkin Method for Modeling Micro-Pulsed Plasma Thrusters*+

G. Lin and G. E. Karniadakis
Division of Applied Mathematics
Brown University
Providence, RI 02912
401-863-1217
glin@cfm.brown.edu, gk@cfm.brown.edu

IEPC-01-154

We present a new numerical method to model micro-pulsed plasma thrusters as a single-fluid/two-temperature plasma flow. A spectral/hp element spatial discretization is employed both for structured and unstructured meshes in two- and three-dimensions. This method is based on a discontinuous Galerkin treatment of the advection and diffusion components, and it is stable in the L_2 sense. Preliminary simulations of MHD flow in two different geometries are presented, and p-refinement is demonstrated that allows higher order accuracy without re-meshing.

Introduction

The pulsed plasma thruster (PPT) has been studied empirically for over thirty years [1]. The thruster's operational simplicity and robustness, allowed for extensive empirical analysis, mainly during the 1960's and 1970's. Renewed interest for small satellite missions has prompted further investigation of PPT behavior in order to achieve improved performance and better insight for scaling operation [2-5].

Micro-PPTs operate the same way as conventional PPTs, i.e. Teflon is ablated and ionized during a pulsed discharge. However, the triggering mechanism may be different and in fact it may not exist at all [6]. A micro-PPT has characteristic dimensions of the order of 1mm, which is one order of magnitude less than even the smallest conventional PPT design. The typical energy discharge is of the order of 1 J, and the ablated material per pulse is about 1 μg. For example, a coaxial micro-PPT fabricated at Edwards AFRL has a 2 mm anode diameter and ablates Teflon mass at a rate of 1.3 μg/pulse [6].

Modeling of thrusters in micro-domain requires a new approach as viscous effects are important and there may be an overlap of electro-dynamic and gas dynamics scales. A combined atomistic-continuum approach is required to address issues associated with non-equilibrium effects, especially for the very small micro-PPT designs. In particular, in addition to the multi-species nature of the flow in PPTs and the coupling with the external circuit and the ablating solid surface, in micro-PPTs we also need to address:

- Continuum, transitional and rarefied regimes.
- Multiple time and length scales.
- Viscous layers and sheath interactions.
- Local non-equilibrium effects.
- Different electric circuits.
- New self-triggering mechanisms.

In this paper we adopt a continuum-based methodology that treats the viscous effects but we have not yet incorporated slip boundary conditions. A high-order boundary condition for velocity slip and temperature jump has been developed in [7] and will be implemented in the context of the continuum approach. Also, a parallel effort at WPI (N. Gatsonis, private communications) is focused on atomistic modeling of micro-PPTs.

---

* Presented as Paper IEPC-01-154 at the 27th International Electric Propulsion Conference, Pasadena, CA, 15-19 October, 2001.

The compressible magneto-hydro-dynamics (MHD) equations describing plasma flow in PPTs are time-dependent. In addition, these equations are strongly coupled and exhibit mixed hyperbolic/parabolic character depending on the parameter range, with a large range of temporal and spatial scales involved. Most of these issues have been adequately addressed in the published works [8-13]. However, one of the limitations of the current numerical methods is that they are of low-order accurate. High-order accuracy is important for capturing the inherent transient behavior of PPTs. Moreover, high-order methods are more suitable for resolving small scales in the viscous micro-pulsed plasma thrusters.

Neglecting the inertia contribution from the electrons and considering that ions and electrons have different temperatures, the plasma flow can be modeled as a single-fluid/two-temperature problem. The imposition of the divergence-free condition for the magnetic field results in a loss of the hyperbolicity of the ideal MHD equations. The development of suitable Riemann solvers by Powell [11] can be easily extended to multi-dimensions and also to high-order discretization.

In the following, we first formulate the discontinuous Galerkin method for the advection and diffusion equations. Then, we present the specific algorithms for the MHD equations. Subsequently, we present numerical simulations of MHD flow in micro-PPT in two- and three dimensions. We conclude with a brief summary.

Discontinuous Galerkin Formulation

We present first the discontinuous Galerkin (DG) formulation for a generic system of advection-diffusion equations of the form

$$\vec{U}_t + \nabla \cdot F^{Ideal} = m\nabla \cdot F^{Visc}, \qquad (1)$$

where F^{Ideal} and F^{Ideal} correspond to inviscid and viscous flux contributions, respectively. Specific implementation issues for the MHD system will be discussed separately in the next section. Splitting the advection-diffusion operator in this form allows for a separate treatment of the inviscid and viscous contributions, which in general exhibit different mathematical properities.

Discontinuous Galerkin for Advection

To explain the formulation we consider the linear two-dimensional equation for advection of a conserved quantity u in a region Ω

$$\frac{\partial u}{\partial t} + \nabla \cdot F(u) = 0, \qquad (2)$$

where

$$F(u) = F(u)^{Ideal} = (f(u), g(u))$$

is the flux vector which defines the transport of u(x,t). We start with the variational statement of the standard Galerkin formulation of (2) by multiplying by a test function n and integrating by parts

$$\int_\Omega \frac{\partial u}{\partial t} n\,dx + \int_{\partial\Omega} n\; n \cdot F(u)\,ds - \int_\Omega \nabla n \cdot F(u)\,dx = 0 \qquad (3)$$

where n is the unit normal and F(u) is the flux. In the discontinuous Galerkin formulation, each element (E) is treated separately corresponding to a variational statement (after integrating by parts once more),

$$\frac{\partial}{\partial t}(u,n)_E + \int_{\partial\Gamma_E} n\,(f(u_i,u_e) - F(u_i)) \cdot n\,ds + (\nabla \cdot F(u), n)_E = 0 \qquad (4)$$

Here $f(u_i,u_e)$ is a numerical flux at the interface between elements (e:exterior, i:interior) that is chosen based on upwind considerations. For a system of equations it is obtained using an approximate Riemann solver [14].

Discontinuous Galerkin for Diffusion

The main idea in the discontinuous Galerkin formulation for diffusion is similar to the one in mixed methods [15], i.e., the use of an auxiliary variable.

Here, we consider as a model problem a parabolic equation with variable coefficient $m(x)$ to demonstrate the treatment of the viscous contributions:

$$u_t = \nabla \cdot (m\nabla u) + f, \qquad in\Omega, \quad u \in L^2(\Omega)$$

$$u = g(x,t), \quad on \partial\Omega.$$

We then introduce the flux variable

$$q = -m\nabla u$$

with

$$q(x,t) \in L^2(\Omega),$$

and re-write the parabolic equation

$$u_t = -\nabla \cdot q + f, \qquad in \Omega$$

$$1/mq = -\nabla u, \qquad in\ \Omega$$

$$u = g(x,t), \qquad on \partial\Omega$$

The weak formulation of the problem is then as follows. Find

$$(q,u) \in L^2(\Omega) \times L^2(\Omega)$$

such that

$$(u_t, w)_E = (q, \nabla w)_E - (w, q_b \cdot n)_E + (f, w)_E, \forall w \in L^2(\Omega)$$

$$1/m(q,v)_E = (u, \nabla \cdot v)_E - (u_b, v \cdot n)_E, \quad \forall v \in L^2(\Omega)$$

$$u = g(x,t), \qquad on \partial\Omega$$

By integrating by parts again, we obtain an equivalent formulation, which is easier to implement. The new variational problem is

$$(u_t, w)_E = (-\nabla \cdot q, w)_E - (w, (q_b - q_i) \cdot n)_E + (f, w)_E, \forall w \in L^2(\Omega)$$

$$1/m(q,v)_E = (-\nabla u, v)_E - (u_b - u_i, v \cdot n)_E, \quad \forall v \in L^2(\Omega)$$

$$u = g(x,t), \quad on \partial\Omega$$

Here the subscript (i) denotes contributions evaluated at the interior side of the boundary. The terms at the boundary (denoted by b) are evaluated based on averaging the corresponding values at either side of the element. The above system is currently solved explicitly but iterative solution schemes (implicit) are also under consideration. In space, spectral/hp discretization is employed that involves Jacobi orthogonal polynomials with support on each element [14].

Governing Equations

The single-fluid/two-temperature plasma equations can be expressed in conservative form in compact notation as

$$\frac{\partial r}{\partial t} = -\nabla \cdot (rV)$$

$$\frac{\partial (rV)}{\partial t} = -\nabla \cdot (rVV^t - BB^t + (p + \frac{1}{2}|B|^2)I - \frac{1}{S_v}t)$$

$$\frac{\partial B}{\partial t} = -\nabla \times (B \times V + \frac{1}{S_r}\nabla \times B + \frac{s_o B_o}{ecn_e S_r} J \times B - \frac{s_o B_o}{en_e S_r}\nabla p_e)$$

$$\frac{\partial E_{total}}{\partial t} = -\nabla \cdot ((E_{total} + p)v + (\frac{1}{2}|B|^2 I - BB^t) \cdot v - \frac{1}{S_v}V \cdot t + \frac{1}{S_r}(B \cdot \nabla B - \nabla (B \cdot B)) - \frac{1}{S_v \Pr_e}\nabla T_e - \frac{1}{S_v \Pr_i}\nabla T_i + \frac{s_o B_o}{ecn_e S_r} J \times B - \frac{s_o B_o}{en_e S_r}\nabla p_e) + J \cdot E$$

$$\frac{\partial E_e}{\partial t} = -\nabla \cdot (E_e V + p_e V) + V \cdot \nabla p_e + \frac{1}{S_{ve}} t_e \cdot \nabla V + \nabla \cdot (\frac{1}{S_{ve} \Pr_e}\nabla T_e) + J \cdot E - f_{ei}$$

$$\nabla \cdot B = 0$$

where

$$t = (\partial_j V_i + \partial_i V_j) - \frac{2}{3}\nabla \cdot V d_{ij}$$

$$E_{total} = re_i + re_e + \frac{1}{2}r(U^2 + V^2 + W^2) + \frac{1}{2}(B_x^2 + B_y^2 + B_z^2)$$

And also the Generalized Ohm's Law

$$E = hJ - v \times B + \frac{J \times B}{ecn_e} - \frac{\nabla P_e}{2en_e}$$

Alternatively, in flux form with the explicitly stated fluxes, they are expressed as

$$\frac{\partial U}{\partial t} = -\frac{\partial F_x^{Ideal}}{\partial x} - \frac{\partial F_y^{Ideal}}{\partial y} - \frac{\partial F_z^{Ideal}}{\partial z} + \frac{\partial F_x^{Visc}}{\partial x} + \frac{\partial F_y^{Visc}}{\partial y} + \frac{\partial F_z^{Visc}}{\partial z} + S_{MHD}$$

$$\nabla \cdot B = 0$$

$$U = (\rho,\ \rho u,\ \rho n,\ \rho w,\ B_x,\ B_y,\ B_z,\ E,\ E_e)$$

$$F_x^{Ideal} = (\rho u,\ \rho u^2 - B_x^2 + \bar{p},\ \rho u n - B_x B_y,$$
$$\rho u w - B_x B_z, 0, u B_y - n B_x, u B_z - w B_x,$$
$$(E + \bar{p})u - (v \cdot B) B_x, (E_e + p_e) u)^T$$

$$F_y^{Ideal} = (\rho n, \rho u v - B_y B_x, \rho n^2 - B_{y_y}^2 + \bar{p},$$
$$\rho v w - B_y B_z, v B_x - u B_y, 0, v B_z - w B_y,$$
$$(E + \bar{p}) v - (v \cdot B) B_y, (E_e + p_e) v)^T$$

$$F_z^{Ideal} = (\rho w, \rho u w - B_z B_x, \rho w n - B_z B_y,$$
$$\rho w^2 - B_x^2 + \bar{p}, w B_z - u B_x, w B_y - n B_x, 0,$$
$$(E + \bar{p}) w - (v \cdot B) B_x, (E_e + p_e) w)^T$$

$$F_x^{Visc} = (0, \frac{2}{S_v}(\frac{\partial u}{\partial x} - \frac{1}{3}\nabla \cdot v), \frac{1}{S_v}(\frac{\partial u}{\partial y} + \frac{\partial v}{\partial x}),$$
$$\frac{1}{S_v}(\frac{\partial u}{\partial z} + \frac{\partial w}{\partial x}), 0, \frac{1}{S_r}(\frac{\partial B_y}{\partial x} - \frac{\partial B_x}{\partial y}),$$
$$\frac{1}{S_r}(\frac{\partial B_z}{\partial x} - \frac{\partial B_x}{\partial z}), \frac{1}{S_v}(-\frac{2}{3}(\nabla \cdot v) u + v \cdot \nabla u$$
$$+ \frac{1}{2}\frac{\partial V^2}{\partial x} + \frac{1}{\mathrm{Pr}}\frac{\partial T}{\partial x}) + \frac{1}{Sr}(\frac{1}{2}\frac{\partial(|B|^2)}{\partial x} - B \cdot \nabla B_x), \frac{1}{S_{ve}\,\mathrm{Pr}_e}\frac{\partial T}{\partial x})^T$$

$$F_y^{Visc} = (0, \frac{1}{S_v}(\frac{\partial u}{\partial y} + \frac{\partial v}{\partial x}), \frac{2}{S_v}(\frac{\partial v}{\partial y} - \frac{1}{3}\nabla \cdot v),$$
$$\frac{1}{S_v}(\frac{\partial v}{\partial z} + \frac{\partial w}{\partial y}), \frac{1}{S_r}(\frac{\partial B_x}{\partial y} - \frac{\partial B_y}{\partial x}), 0,$$
$$\frac{1}{S_r}(\frac{\partial B_z}{\partial y} - \frac{\partial B_y}{\partial z}), \frac{1}{S_v}(-\frac{2}{3}(\nabla \cdot v) n + v \cdot \nabla n$$
$$+ \frac{1}{2}\frac{\partial V^2}{\partial y} + \frac{1}{\mathrm{Pr}}\frac{\partial T}{\partial y}) + \frac{1}{Sr}(\frac{1}{2}\frac{\partial(|B|^2)}{\partial y} - B \cdot \nabla B_y), \frac{1}{S_{ve}\,\mathrm{Pr}_e}\frac{\partial T}{\partial y})^T$$

$$F_z^{Visc} = (0, \frac{1}{S_v}(\frac{\partial u}{\partial z} + \frac{\partial w}{\partial x}), \frac{1}{S_v}(\frac{\partial w}{\partial y} + \frac{\partial n}{\partial z}), \frac{2}{S_v}(\frac{\partial w}{\partial z} - \frac{1}{3}\nabla \cdot v),$$
$$\frac{1}{S_r}(\frac{\partial B_x}{\partial z} - \frac{\partial B_z}{\partial x}), \frac{1}{S_r}(\frac{\partial B_y}{\partial z} - \frac{\partial B_z}{\partial y}),$$
$$0, \frac{1}{S_v}(-\frac{2}{3}(\nabla \cdot v) w + v \cdot \nabla w$$
$$+ \frac{1}{2}\frac{\partial V^2}{\partial z} + \frac{1}{\mathrm{Pr}}\frac{\partial T}{\partial z}) + \frac{1}{Sr}(\frac{1}{2}\frac{\partial(|B|^2)}{\partial z} - B \cdot \nabla B_z), \frac{1}{S_{ve}\,\mathrm{Pr}_e}\frac{\partial T}{\partial z})^T$$

$$S_{MHD} = (0,0,0,0,0,0,0, (J \times E), (V \cdot \nabla p_e + \frac{1}{S_{ve}} t_e \cdot \nabla V + J \times E - f_{ei}))$$

where

$$E_{total} = \frac{p}{(g-1)} + \frac{1}{2}(\rho V \cdot V + B \cdot B)$$

$$\bar{p} = p + \frac{1}{2} B \cdot B$$

$$\mathrm{Pr} = \frac{c_p m}{k}$$

$$S_v = \frac{\rho_0 V_A L_0}{m}$$

$$S_r = \frac{V_A L_0}{h}$$

$$V_A^2 = \frac{B \cdot B}{\rho}$$

$$A = \sqrt{V_A^2 / V_0^2}$$

The $\nabla \cdot B = 0$ Constraint

The presence of the $\nabla \cdot \mathrm{B} = 0$ constraint implies that the equations do not have a strictly hyperbolic character. It has been shown in [16] that even a small divergence in the magnetic fields can dramatically change the character of results from numerical simulations. Here we follow the formulation of Powell [11]. For a single temperature, the idea is to re-formulate the Jacobian matrix to include an "eighth-wave", i.e. the divergent mode that corresponds to velocity u. In this way, the degeneracy associated with the divergence-free condition is avoided; the rest of the eigenvalues of the Jacobian remain the same. This modification effectively corresponds to adding to the MHD equations a source term proportional to $\nabla \cdot B = 0$,

$$S_{powell} = -(\nabla \cdot B)(0, B_x, B_y, B_z, u, v, w, v \cdot B)^T$$

to the right-hand-side of the evolution equation. For the current formulation with *two different temperatures* for the ions and electrons we need two extra waves so the total number of eigenvalues is nine.

Implementation of the Inviscid Flux Terms

We evaluate the inviscid fluxes and their derivatives in the interior of the elements and add correction

terms for the discontinuities in the flux between any two adjacent elements as discussed in subsection 2.1. In order to evaluate the inviscid flux at an element interface we use one-dimensional Riemann solvers to supply a numerical flux there. At a domain boundary we use the specified conditions and treat the exterior boundary as the boundary of a "ghost" element. This way we can use the same Riemann solver at all element boundaries.

We linearize the one-dimensional flux F_n^{Ideal} in the normal direction to a shared element-boundary using the average of the state vector at either side of the element boundary. That is, since F_n^{Ideal} is a nonlinear function of the state vector we use the average state to form an approximation to the Jacobian of the flux vector A_c. The Jacobian matrix for the flux vector for the evolution equations expressed in primitive variables is simpler than the conserved form. Thus, we perform the linearization for the primitive form and transform to the conserved form. The primitive Jacobian matrix A_p is 9x9 and has the form

$$\begin{bmatrix} u & \rho & 0 & 0 & 0 & 0 & 0 & 0 & 0 \\ 0 & u & 0 & 0 & -\frac{B_x}{\mu\rho} & \frac{B_y}{\mu\rho} & \frac{B_z}{\mu\rho} & \frac{1}{\mu\rho} & 0 \\ 0 & 0 & u & 0 & -\frac{B_y}{\mu\rho} & \frac{B_x}{\mu\rho} & 0 & \frac{1}{\mu\rho} & 0 \\ 0 & 0 & 0 & u & -\frac{B_z}{\mu\rho} & 0 & \frac{B_x}{\mu\rho} & 0 & 0 \\ 0 & 0 & 0 & 0 & 0 & 0 & 0 & 0 & 0 \\ 0 & B_y & -B_x & 0 & -v & u & 0 & 0 & 0 \\ 0 & B_z & 0 & -B_x & -w & 0 & u & 0 & 0 \\ 0 & \gamma p & 0 & 0 & -(\gamma-1)u\cdot B & 0 & 0 & u & 0 \\ 0 & \gamma_e p_e & 0 & 0 & 0 & 0 & 0 & 0 & u \end{bmatrix}$$

The scaled left- and right-eigenvectors of the primitive Jacobian matrix A_p, due to Powell [11], are

Entropy wave,

$$\lambda_e = u$$

$$l_e = (1,0,0,0,0,0,0,-\frac{1}{a^2},0)$$

$$r_e = (1,0,0,0,0,0,0,0,0)^t$$

Alfven waves

$$\lambda_a = u \pm \frac{B_x}{\sqrt{\mu\rho}}$$

$$l_e = \frac{1}{\sqrt{2}}(0,0,-\beta_z,\beta_y,\pm\frac{\beta_z}{\sqrt{\mu\rho}},\mp\frac{\beta_y}{\sqrt{\mu\rho}},0,0)$$

$$r_e = \frac{1}{\sqrt{2}}(0,0,-\beta_z,\beta_y,0,\pm\beta_z\sqrt{\mu\rho},\mp\beta_y\sqrt{\mu\rho},0,0)^t$$

Fast waves

$$\lambda_a = u \pm C_s$$

$$l_e = \frac{1}{2a^2}(0,\pm\alpha_s C_s,\pm\alpha_f C_f \beta_x \beta_y,\pm\alpha_f C_f \beta_x \beta_z,0,$$
$$-\frac{\alpha_f \beta_y a}{\sqrt{\mu\rho}},-\frac{\alpha_f \beta_z}{\sqrt{\mu\rho}},\frac{\alpha_s}{\mu\rho},0)$$

$$r_e = (\mu\rho\alpha_s,\pm\alpha_s C_s,\pm\alpha_f C_f \beta_x \beta_y,\pm\alpha_f C_f \beta_x \beta_z,0,$$
$$-\alpha_f \beta_y a\sqrt{\mu\rho},-\alpha_f \beta_z a\sqrt{\mu\rho},\alpha_s\gamma p,\alpha_s\gamma_e p_e)^t$$

Compared to [11], we have an extra (ninth) wave, which corresponds to the electron energy:

$$l_{ee} = (0,0,0,0,0,0,0,0,1)$$

$$r_{ee} = (-\frac{\gamma_e p_e}{\mu\rho},0,0,0,0,0,0,0,1)^t$$

where:

$$(a^*)^2 = \frac{\gamma p + B\cdot B}{\mu\rho}$$

$$C_f^2 = \frac{1}{2}((a^*)^2 + \sqrt{(a^*)^4 - 4\frac{\gamma p B_x^2}{\mu\rho^2}})$$

$$C_s^2 = \frac{1}{2}((a^*)^2 - \sqrt{(a^*)^4 - 4\frac{\gamma p B_x^2}{\mu\rho^2}})$$

$$\alpha_f^2 = \frac{a^2 - C_s^2}{C_f^2 - C_s^2}$$

$$\alpha_s^2 = \frac{C_f^2 - a^2}{C_f^2 - C_s^2}$$

$$\beta_x = \mathrm{sgn}(B_x)$$

$$\beta_y = \frac{B_y}{\sqrt{B_y^2 + B_z^2}}$$

$$\beta_z = \frac{B_z}{\sqrt{B_y^2 + B_z^2}}$$

We can transform between the primitive and conserved variables with the following transform

$$A_c = \frac{\partial U}{\partial W} A_p \frac{\partial W}{\partial U}$$

where

$$U = (\rho, \rho u, \rho v, \rho w, B_x, B_y, B_z, E, E_e)$$

are the conserved variables and

$$W = (\rho, u, v, w, B_x, B_y, B_z, p, p_e)$$

are the primitive variables. This gives:

$$\frac{\partial U}{\partial W} = \begin{bmatrix} 1 & 0 & 0 & 0 & 0 & 0 & 0 & 0 & 0 \\ u & \rho & 0 & 0 & 0 & 0 & 0 & 0 & 0 \\ v & 0 & \rho & 0 & 0 & 0 & 0 & 0 & 0 \\ w & 0 & 0 & \rho & 0 & 0 & 0 & 0 & 0 \\ 0 & 0 & 0 & 0 & 1 & 0 & 0 & 0 & 0 \\ 0 & 0 & 0 & 0 & 0 & 1 & 0 & 0 & 0 \\ 0 & 0 & 0 & 0 & 0 & 0 & 1 & 0 & 0 \\ \frac{u \cdot u}{2} & \rho u & \rho v & \rho w & B_x & B_y & B_z & \frac{1}{\gamma - 1} & 0 \\ 0 & 0 & 0 & 0 & 0 & 0 & 0 & 0 & \frac{1}{\gamma_e - 1} \end{bmatrix}$$

And

$$\begin{bmatrix} u & \rho & 0 & 0 & 0 & 0 & 0 & 0 & 0 \\ 0 & u & 0 & 0 & -\frac{B_x}{\rho} & \frac{B_y}{\rho} & \frac{B_z}{\rho} & \frac{1}{\rho} & 0 \\ 0 & 0 & u & 0 & -\frac{B_y}{\rho} & \frac{B_x}{\rho} & 0 & \frac{1}{\rho} & 0 \\ 0 & 0 & 0 & u & -\frac{B_z}{\rho} & 0 & \frac{B_x}{\rho} & 0 & 0 \\ 0 & 0 & 0 & 0 & 0 & 0 & 0 & 0 & 0 \\ 0 & B_y & -B_x & 0 & -v & u & 0 & 0 & 0 \\ 0 & B_z & 0 & -B_x & -w & 0 & u & 0 & 0 \\ 0 & \gamma p & 0 & 0 & -(\gamma - 1) u \cdot B & 0 & 0 & u & 0 \\ 0 & \gamma_e p_e & 0 & 0 & 0 & 0 & 0 & 0 & u \end{bmatrix}$$

where

$$\bar{\gamma} = \gamma - 1 \quad , \quad \bar{\gamma}_e = \gamma_e - 1 .$$

We are now in a position to evaluate the numerical flux at the element boundaries. We use the following formulation for the upwinded flux:

$$\hat{F}(U_I, U_E) = \frac{1}{2}(F(U_I) + F(U_E) - \frac{\partial U}{\partial W} \sum_{k=1}^{k=9} \alpha_k |l_k| r_k) \qquad (5)$$

$$\alpha_k = l_k \cdot \frac{\partial W}{\partial U}(U_E - U_I) \qquad (6)$$

Here the l_k and r_k are the ordered left and right eigenvectors of the primitive Jacobian matrix. We have to apply the $\frac{\partial U}{\partial W}$ operator to the right eigenvectors to calculate the conserved flux. The λ_k is the wave speeds associated with the eigenvector.

Implementation of the Viscous Terms

The viscous terms are evaluated in two steps. First, we obtain the spatial derivatives of the primitive variables using the discontinuous Galerkin approach. Then, we repeat the process for each of the viscous fluxes using these derivatives. Dirichlet boundary conditions for the momentum and energy characteristic variables can be imposed weakly or explicitly after the fluxes have been evaluated and then project the result using the orthogonal Jacobi polynomial basis.

Numerical Simulations

Micro-PPT modeled with two species MHD pulsed inflow

First we consider a two-dimensional model problem that is similar to the micro-PPT proposed in [6]. Specifically, we have developed our two-dimensional MHD code to be able to deal with time-dependent boundary conditions for all variables. The boundary conditions after normalization are

Inflow :

$$\rho = 3.0 + 2\sin^2(\pi t)$$
$$u = 1.0, \quad v = 0$$
$$B_x = 0.1, \quad B_y = 0$$

$$T = 7.14$$

$$E_{total} = \rho T + \frac{1}{2}(B_x^2 + B_y^2) + \frac{1}{2}\rho(u^2 + v^2)$$

$$E_{electron} = \frac{1}{2}\rho T$$

The corresponding initial conditions after normalization are:

$$\rho = 1.0$$

$$u = 1.0, \quad v = 0$$

$$B_x = 0.1, \quad B_y = 0$$

$$T = 7.14$$

$$E_{total} = \rho T + \frac{1}{2}(B_x^2 + B_y^2) + \frac{1}{2}\rho(u^2 + v^2)$$

$$E_{electron} = \frac{1}{2}\rho T$$

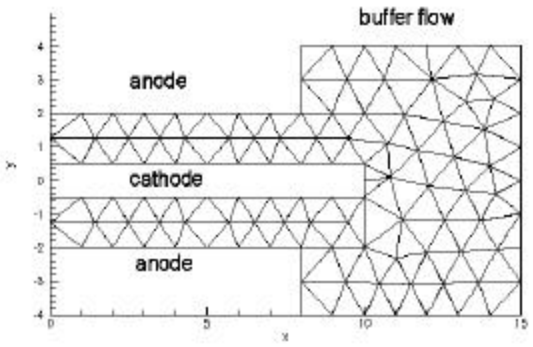

Figure 1 - Unstructured mesh for PPT model with two species MHD and pulsed inflow.

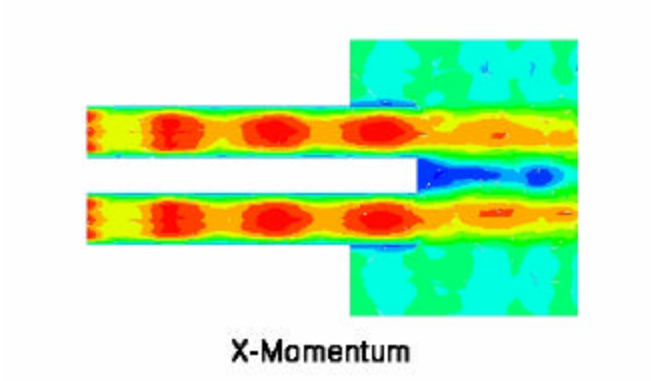

Figure 2 - Momentum in streamwise direction.

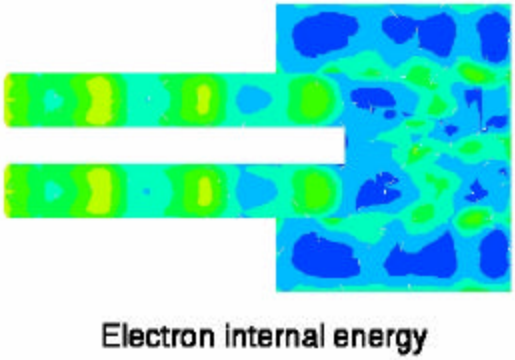

Figure 3 - Electron internal energy in two species MHD and pulsed inflow.

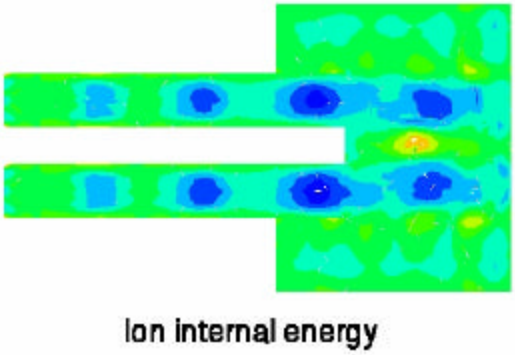

Figure 4 - Ion internal energy in two species MHD and pulsed inflow.

In figure 1, we show the unstructured mesh with a buffer region. The polynomial order used in each element is $p = 4$. In figure 2,3 and 4, we show typical results of the several pulses.

Two- and three-dimensional MHD flows in LES/6 PPT

Here we consider the LES/6 PPT geometry; see reference [17] for dimensions.

Two-dimensional MHD flow in Micro-PPT (LES/6)

The mesh we employed in the two-dimensional simulations is shown in Figure 5. The boundary conditions we employ are:

Inflow:

$$\rho = 1.36 \times 10^{-2} kg/m^3$$

$$B_x = 0(T), \quad B_{z,\inf low} = 0.001225\ \mu_0 j_0$$

where:

$$\mu_0 = 4\pi \times 10^{-7}\frac{H}{m},\ \sigma_0 = 1.32\times 10^4 \frac{1}{\Omega m},$$

$$V_0 = 1360V,\ j_0 = \sigma_0 \frac{V_0}{h}, h = 0.03m$$

$$T = 600K,$$

$$u = U_s = \sqrt{\gamma RT}, \quad w = 0$$

$$E_{total} = \frac{\rho RT}{\gamma - 1} + \frac{1}{2\mu_0}(B_x^2 + B_z^2) + \frac{1}{2}\rho(u^2 + w^2)$$

Outflow:

$$\rho = 1.36\times 10^{-5}\ \mathrm{kg/m^3}$$

$$B_x = 0(T),$$

$$B_{z,outflow} = \sigma B_{z,inlow} \quad (\sigma \le 0.1)$$

$$T = 600K,$$

$$u = xU_s \quad (x > 1), \quad w = 0$$

$$E_{total} = \frac{\rho RT}{\gamma - 1} + \frac{1}{2\mu_0}(B_x^2 + B_z^2) + \frac{1}{2}\rho(u^2 + w^2)$$

We employed the following initial conditions:

$$\rho = \begin{cases} 1.36\times 10^{-2} kg/m^3 & x \le 0.00245m \\ 1.36\times 10^{-5} kg/m^3 & 0.00245m < x \le 0.06m \end{cases}$$

$$B_z = \begin{cases} \mu_0 j_0 x(T) & 0m \le x \le 0.00245m \\ 0.00245\mu_0 j_0 \dfrac{0.006 - x}{0.006 - 0.00245}(T) & 0.00245m < x \le 0.006m \\ 0(T) & 0.006m < x \le 0.06m \end{cases}$$

where:

$$\mu_0 = 4\pi \times 10^{-7}\frac{H}{m},\ \sigma_0 = 1.32\times 10^4 \frac{1}{\Omega m},$$

$$V_0 = 1360V,\ j_0 = \sigma_0 \frac{V_0}{h}, h = 0.03m$$

$$B_x = 0$$

$$T = \begin{cases} 600K & x = 0m, or, 0.06m \\ 10000K & 0m < x < 0.06m \end{cases}$$

$$u = w = 0m/s$$

$$E_{total} = \frac{\rho RT}{\gamma - 1} + \frac{1}{2\mu_0}(B_x^2 + B_z^2) + \frac{1}{2}\rho(u^2 + w^2)$$

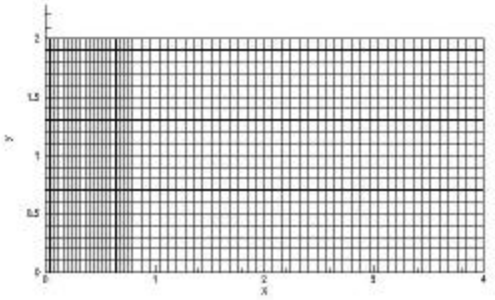

Figure 5 - Structured mesh for two-dimensional PPT (LES/6) model.

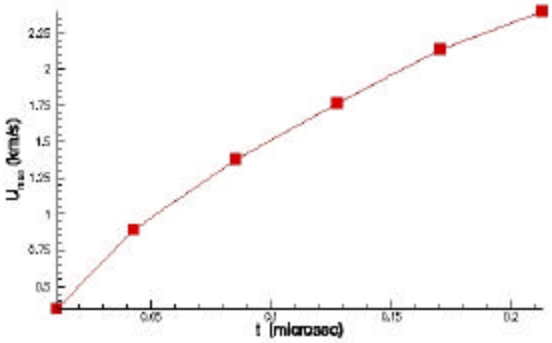

Figure 6 - PPT (LES/6) model initial acceleration.

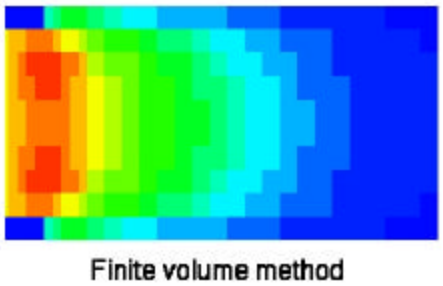

Figure 7 - Streamwise velocity in PPT(LES/6) using finite volume method.

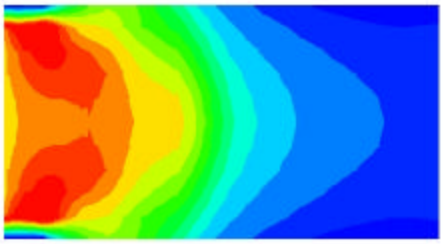

Figure 8 – Streamwise velocity in PPT(LES/6) using second-order spectral/hp element method.

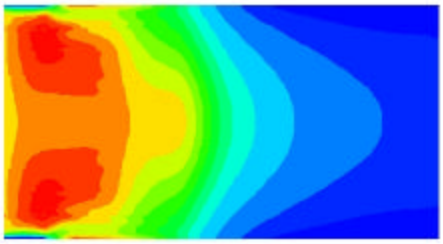

Figure 9 - Streamwise velocity in PPT(LES/6) using fourth-order spectral/hp element method.

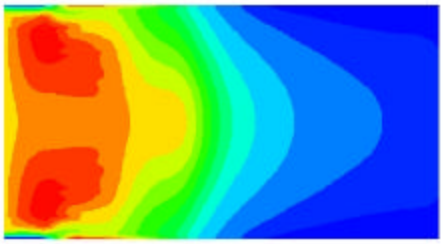

Figure 10 - Streamwise velocity in PPT(LES/6) using sixth-order spectral/hp element method.

In Figure 6 we show the initial acceleration obtained in this simulation of LES/6. Figures 7 to 10 show successive p-refinement, i.e. the order of the Jacobi polynomial is increased without change of the mesh of Figure 5. We see that the solution is improved significantly and beyond fourth-order we have full convergence. Note that this is not trivial given the fact that we deal with a flow with shocks and very steep gradients, which conventional spectral methods cannot handle. However, the discontinuous Galerkin method is stable in the L_2 norm and no explicit limiting or artificial diffusion is required to obtain these results.

Three-dimensional MHD flow in Micro-PPT (LES/6)

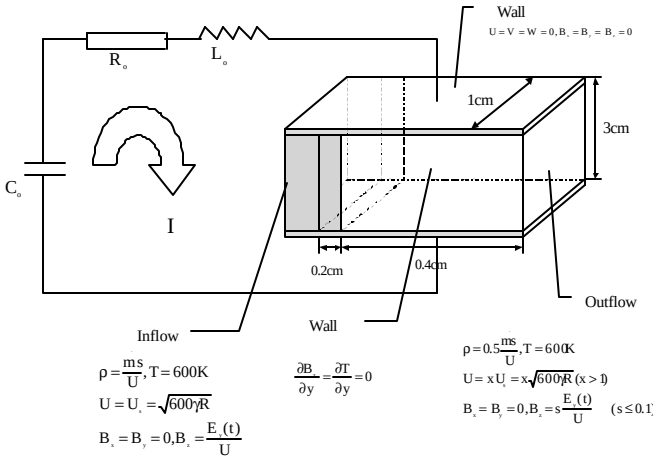

Figure 11 – Sketch of the three-Dimensional PPT (LES/6), and boundary conditions.

Next we simulate the three-dimensional LES/6 PPT shown in Figure 11. The corresponding structured mesh is shown in Figure 12.

The boundary conditions we use are:

Inflow:

$$\rho = 1.36\times10^{-2}\, kg/m^3$$

$$B_x = B_y = 0(T)$$

$$B_z = 0.001225\mu_0 j_0$$

where:

$$\mu_0 = 4\pi\times10^{-7}\frac{H}{m},\ \sigma_0 = 1.32\times10^{4}\frac{1}{\Omega m},$$

$$V_0 = 1360V,\ j_0 = \sigma_0\frac{V_0}{h},\ h = 0.03m$$

$$T = 600\,K$$

$$u = U_s = \sqrt{\gamma RT},\quad v = w = 0$$

$$E_{total} = \frac{\rho RT}{\gamma - 1} + \frac{1}{2\mu_0}(B_x^2 + B_y^2 + B_z^2)$$
$$+\frac{1}{2}\rho(u^2 + v^2 + w^2)$$

Outflow:

$$\rho = 1.36\times10^{-5}\,kg/m^3$$

$$B_x = B_y = 0(T)$$

$$B_{z,outflow} = sB_{z,inlow} \quad (s \le 0.1)$$

$$T = 600\,K$$

$$u = xU_s \quad (x > 1), \quad v = w = 0$$

$$E_{total} = \frac{\rho RT}{\gamma - 1} + \frac{1}{2\mu_0}(B_x^2 + B_y^2 + B_z^2) + \frac{1}{2}\rho(u^2 + v^2 + w^2)$$

The initial conditions we employ are:

$$\rho = \begin{cases} 1.36\times10^{-2}\,kg/m^3 & x \le 0.00245\,m \\ 1.36\times10^{-5}\,kg/m^3 & 0.00245\,m < x \le 0.06m \end{cases}$$

$$B_z = \begin{cases} \mu_0 j_0 x\,(T) & 0m \le x \le 0.00245m \\ 0.00245\mu_0 j_0 \dfrac{0.006 - x}{0.006 - 0.00245}(T) & 0.00245m < x \le 0.006m \\ 0\,(T) & 0.006m < x \le 0.06m \end{cases}$$

Where:

$$\mu_0 = 4\pi\times10^{-7}\frac{H}{m}, \sigma_0 = 1.32\times10^4\frac{1}{\Omega m},$$

$$V_0 = 1360V, j_0 = \sigma_0\frac{V_0}{h}, h = 0.03m$$

$$B_x = B_y = 0$$

$$T = \begin{cases} 600\,K & x = 0m, or, 0.06m \\ 10000\,K & 0m < x < 0.06m \end{cases}$$

$$u = v = w = 0m/s$$

$$E_{total} = \frac{\rho RT}{\gamma - 1} + \frac{1}{2}\rho(u^2 + v^2 + w^2) + \frac{1}{2\mu_0}(B_x^2 + B_y^2 + B_z^2)$$

In Figures 12 and 13 we plot instantaneous contours of the streamwise velocity and the total energy from these preliminary simulations.

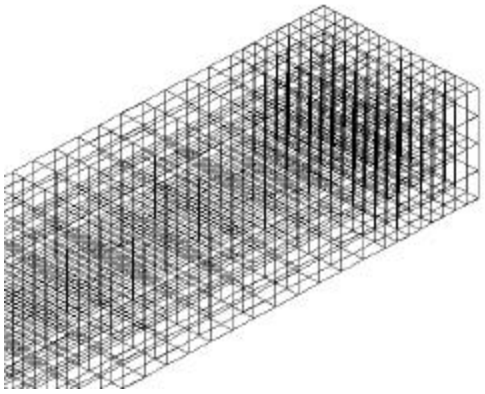

Figure 12 - Structured mesh for three-dimensional PPT (LES/6) model.

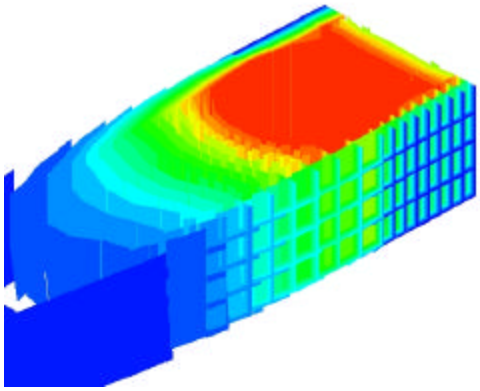

Figure 13 - Stream wise velocity in three-dimensional PPT (LES/6) model.

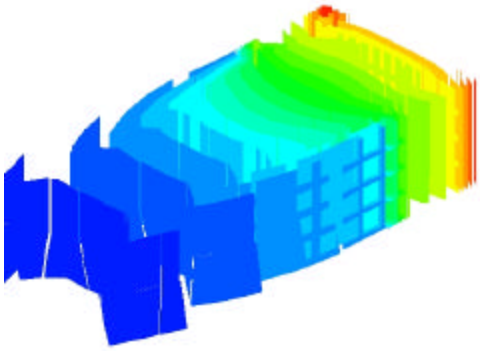

Figure 14 - Total energy in three-dimensional PPT (LES/6) model.

Summary

We have presented a high-order method to model viscous MHD formulated for a single fluid but two separate temperatures (ions and electrons). In this work we have shown qualitatively how the method works and how p-refinement (i.e. spectral refinement) can lead to high accuracy even in the presence of very steep gradients and even shocks. In future work we will couple the MHD solver to an ablation model and the external circuit, and we will implement velocity slip and temperature jump as boundary conditions. These additions are necessary in order to provide meaningful quantitative information that may aid the design of micro-PPTs.

Acknowledgements

This work was supported by the Computational Mathematics program of AFOSR. Computations were performed at NPACI's and Brown's IBM SP3. We would like to thank Prof. N. Gatsonis of WPI for very useful suggestions regarding this work.

References

[1] A. Solbes and R.J. Vondra, "Performance study of a solid fuel-pulsed electric microthruster," J. Spacecraft, 10 (6), 1973.

[2] H. Kamhawi and P.J. Turchi, "Design, operation, and investigation of an inductively-driven pulsed plasma thruster," AIAA 98-3804, 34th AIAA/ASME/SAE/ASEE Joint Propulsion Conference & Exhibit, July 13-15, 1998, Cleveland, OH.

[3] P.J. Turch, I.G. Mikelides, P.G. Mikelides and H. Kamhawi, "Optimization of pulsed plasma thrusters for microsatellite propulsion," AIAA-99-2301, 35th AIAA/ASME/SAE/ASEE Joint Propulsion Conference & Exhibit, 20-24 June 1999, Los Angeles, CA.

[4] C.A. Scharlemann, R. Corey, I.G. Mikelides, P.J. Turchi and P.G. Mikelides, "Pulsed plasma thrusters variations for improved mission capabilities," AIAA-00-3260, 36th AIAA/ASME/SAE/ASEE Joint Propulsion Conference & Exhibit, 16-19 July 2000, Huntsville, Alabama.

[5] H. Kamhawi, P.J. Turch, P.G. Mikelides and I.G. Mikelides, "Experimental and theoretical investigation of an inverse-pinch coaxial pulsed plasma thruster," AIAA-00-3261, 36th AIAA/ASME/SAE/ASEE Joint Propulsion Conference & Exhibit, 16-19 July 2000, Huntsville, Alabama

[6] F.S. Gulczinski, M.J. Dulligan, J.P. Lake and G.G. Spanjers, "Micropropulsion research at AFRL," AIAA 2000-3255, 38th Joint Propulsion Conference & Exhibit, 16-19 July 2000, Huntsville, Alabama.

[7] G.E. Karniadakis and A. Beskok, Micro Flows: Fundamentals and Simulation, Springer, 2001.

[8] W. Dai and P.R. Woodward, "A simple Riemann solver and high-order Godunov schemes for hyperbolic systems of conservation laws," J. Comput. Phys. 121,51 (1995).

[9] A. L. Zachary, A. Malagoli, and P. Colella, "A higher-order Godunov method for multidimensional ideal magnetohydrodynamics," SIAM J. Sci. Stat Comp. 15 (1994)

[10] R.E.Peterkin, M.H.Frese, and C.R.Sovinec, "Transport magnetic flux in an arbitrary coordinate ALE code," J. Comput. Phys. 140,148 (1998)

[11] K.G.Powell, "An Approximate Riemann Solver for Magnetohydrodynamics," Technical Report ICASE Report 94-24, ICASE, NASA Langley, 1994.

[12] O.S. Jones, U. Shumlak, and D.S. Eberhardt, "An implicit scheme for nonideal magnetohydrodynamics," J. Comput. Phys. 130,231 (1997)

[13] P.Colella, M.Dorr, and D.D. Wake, "A Conservative Finite Difference Method for the Numerical Solution of Plasma Fluid Eequations," Technical Report UCRL-JC-129912, Lawrence Livermore National Laboratory, 1998.

[14] T.C. Warburton and G.E. Karniadakis, "A Discontinuous Galerkin Method for the Viscous MHD Equations," J. Comput. Phys. 152,608-641 (1999)

[15] V. Girault and P. A. Raviart, Finite Element Methods for Navier-Stokes Equations (Springer-Verlag, New York/Berlin, 1986).

[16] J.U. Brackbill and D.C. Barnes, "The effect of nonzero divergence on the numerical solution of the magnetohydrodynamic equations," J. Comput. Phys. 35,426 (1980).

[17] P.G.Mikellides and P.J. Turchi, "Modeling of late-time ablation in Teflon pulsed plasma thrusters," AIAA 96-2733, 32nd AIAA/ASME/SAE/ASEE Joint Propulsion Conference & Exhibit, July 1-3, 1996, Buena Vista, FL.